

Some computational aspects of elastic-plastic large strain analysis

Citation for published version (APA):

Nagtegaal, J. C., & Jong, de, J. E. (1981). Some computational aspects of elastic-plastic large strain analysis. *International Journal for Numerical Methods in Engineering*, 17(1), 15-41.
<https://doi.org/10.1002/nme.1620170103>

DOI:

[10.1002/nme.1620170103](https://doi.org/10.1002/nme.1620170103)

Document status and date:

Published: 01/01/1981

Document Version:

Publisher's PDF, also known as Version of Record (includes final page, issue and volume numbers)

Please check the document version of this publication:

- A submitted manuscript is the version of the article upon submission and before peer-review. There can be important differences between the submitted version and the official published version of record. People interested in the research are advised to contact the author for the final version of the publication, or visit the DOI to the publisher's website.
- The final author version and the galley proof are versions of the publication after peer review.
- The final published version features the final layout of the paper including the volume, issue and page numbers.

[Link to publication](#)

General rights

Copyright and moral rights for the publications made accessible in the public portal are retained by the authors and/or other copyright owners and it is a condition of accessing publications that users recognise and abide by the legal requirements associated with these rights.

- Users may download and print one copy of any publication from the public portal for the purpose of private study or research.
- You may not further distribute the material or use it for any profit-making activity or commercial gain
- You may freely distribute the URL identifying the publication in the public portal.

If the publication is distributed under the terms of Article 25fa of the Dutch Copyright Act, indicated by the "Taverne" license above, please follow below link for the End User Agreement:

www.tue.nl/taverne

Take down policy

If you believe that this document breaches copyright please contact us at:

openaccess@tue.nl

providing details and we will investigate your claim.

SOME COMPUTATIONAL ASPECTS OF ELASTIC-PLASTIC LARGE STRAIN ANALYSIS

J. C. NAGTEGAAL†

MARC Analysis Research Corporation, Rijswijk, The Netherlands

J. E. DE JONG

Philips Research Laboratories, Eindhoven, The Netherlands

SUMMARY

The governing equations for large strain analysis of elastic-plastic problems are reconsidered. An improved form of these equations is derived, which is valid for small increments of strain and large increments of rotation. Special attention is paid to the integration procedures for these equations in the deformation history. It is shown that the tangent modulus procedure for integration of the constitutive equations is conditionally stable, and that implicit methods, such as the 'mean normal' method, are to be preferred. A novel procedure is introduced for the treatment of nonlinear geometric effects. The performance of various element types is examined, with specific attention to effects of 'locking' and distortion. Several applications are discussed to illustrate the various aspects of the formulation developed in this paper.

INTRODUCTION

In recent years, growing interest has been shown in the analysis of metal-forming problems by the finite element method. Initially, attention was focused on the steady-state analysis of continuous processes, such as wire drawing and extrusion. In the analysis of such problems the material behaviour is often assumed to be rigid-perfectly plastic, and an Eulerian flow-type approach is used to formulate the problem.^{1,2} Although reasonably accurate results can be obtained with this method, problems arise when either free boundaries are present or when significant hardening effects occur. Furthermore, the method is not suitable for non steady-state problems or for problems in which the elasticity effects are of importance. For such problems, a Lagrangian-type large deformation formulation is more suitable. One of the first attempts to use such a formulation was made by Hibbitt, Marçal and Rice.³ They used a total Lagrangian formulation, which still causes some problems, since the rate equations of plasticity are most suitably formulated with reference to the current state, and not with reference to the original state.

Later, McMeeking and Rice⁴ pioneered the use of an updated Lagrange-type approach, showing that it was viable for a variety of problems. The updated Lagrange analysis procedure is more suitable for plasticity problems, because at each instant the reference state is updated to coincide with the current state, and this procedure is used here. The governing equations used here are the same as in many other studies where the updated Lagrange method is used. The main contribution of this study is the review of the basic equations with special attention to the

† Currently Technical University, Eindhoven, The Netherlands.

complicating aspects of discretized analysis models. As will be seen, a close study of the effects of discretizing both in space and (deformation) history yields considerably improved analysis procedures with respect to both cost and accuracy.

A difference compared with previously described methods is the derivation of the governing equations directly in incremental form instead of first deriving the rate equations and then generalizing these to a finite increment. This leads to an improved formulation when large increments in rotation occur.

Consideration is given to the type of forward integration method used, with specific attention to the integration of the constitutive equations. It became clear, and was proved, that the usual tangent modulus method for elastic-plastic material behaviour is only stable when the strain increments are relatively small. Several procedures are discussed for the treatment of the geometric nonlinearities, and a novel procedure, called the 'strain correction' method, is developed. Another important aspect of the analysis of forming processing with the updated Lagrange method is the selection of appropriate element types. The results of several comparative calculations indicate that simple elements with relatively few dilatational degrees-of-freedom (to prevent 'locking' of the mesh⁵) give the best performance. The formulation derived in this paper was implemented in the MARC general-purpose nonlinear finite element computer program.⁶ It is intended to serve as a tool in the analysis of actual manufacturing processes. In the final section two examples are presented to illustrate the use of the program in the analysis of some practical problems.

THE UPDATED LAGRANGE PROCEDURE

The incremental procedure of analysis, known as the updated Lagrange procedure, is based upon the following concepts:

1. During each analysis increment a Lagrangian formulation is used: the state variables are defined with respect to the state at the start of the increment.
2. At the end of each increment, the state variables are redefined (updated) with respect to the state at the end of the increment.

First the state at the start of the increment is considered. In the Lagrangian description, the spatial position of a body expressed in terms of a Cartesian co-ordinate system is described by the expression

$$X_i = X_i(\theta^\alpha) \quad (1)$$

where a material point of the body is uniquely defined by its values in the convected curvilinear co-ordinate system θ^α (Figure 1). The equilibrium of the body is expressed by the virtual work equation formulated in terms of the components in the Cartesian co-ordinate system:

$$\int_V \sigma_{ij} \delta \varepsilon_{ij} dV = \int_S P_i \delta u_i dS \quad (2a)$$

or alternatively formulated in terms of the components in the convected curvilinear co-ordinate system:

$$\int_V \sigma^{\alpha\beta} \delta \varepsilon_{\alpha\beta} dV = \int_S P_i \delta u_i dS \quad (2b)$$

For brevity, only surface loads formulated in terms of the Cartesian co-ordinates have been considered. Since the integrations in (2b) are carried out over the current state of the body, the

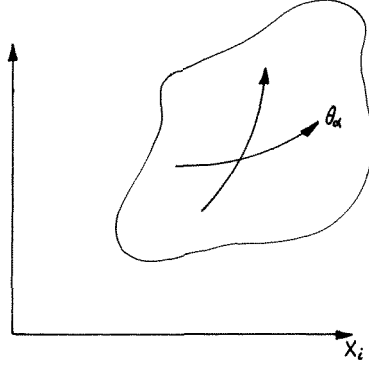


Figure 1. Spatial and material co-ordinate system

contravariant components of Cauchy stress $\sigma^{\alpha\beta}$ are equal to the contravariant components of the second Piola–Kirchhoff stress $S^{\alpha\beta}$. The covariant components of the variations in strain $\delta\varepsilon_{\alpha\beta}$ are related to the Cartesian components of the variations in displacement through

$$\delta\varepsilon_{\alpha\beta} = \frac{1}{2}(X_{k,\alpha} \delta u_{k,\beta} + X_{k,\beta} \delta u_{k,\alpha}) \quad (3)$$

Using the symmetry of $\sigma^{\alpha\beta}$, the virtual work equation can be written as

$$\int_V S^{\alpha\beta} X_{k,\alpha} \delta u_{k,\beta} dV = \int_S P_i \delta u_i dS \quad (4)$$

At the end of the increment, the spatial position of the body is described by a different function of the convected co-ordinates, with the incremental displacement function as the difference:

$$x_i = x_i(\theta^\alpha) = X_i(\theta^\alpha) + \Delta u_i(\theta^\alpha) \quad (5)$$

The virtual work (=equilibrium) equation at the end of the increment takes the form

$$\int_V (S^{\alpha\beta} + \Delta S^{\alpha\beta}) \delta E_{\alpha\beta} dV = \int_S (P_i + \Delta P_i) \delta u_i dS \quad (6)$$

and the variations in Green's strain $\delta E_{\alpha\beta}$ are related to the variations in displacement by

$$\delta E_{\alpha\beta} = \frac{1}{2}(X_{k,\alpha} + \Delta u_{k,\alpha}) \delta u_{k,\beta} + (X_{k,\beta} + \Delta u_{k,\beta}) \delta u_{k,\alpha} \quad (7)$$

Note that the integrations in (6) are still carried out with respect to the state of the body at the start of the increment and that $\Delta S^{\alpha\beta}$ is therefore the increment in the second Piola–Kirchhoff stress.

Using the symmetry of $S^{\alpha\beta}$ and $\Delta S^{\alpha\beta}$, one finds the equilibrium equation expressed in the displacements:

$$\int_V (S^{\alpha\beta} + \Delta S^{\alpha\beta})(X_{k,\alpha} + \Delta u_{k,\alpha}) \delta u_{k,\beta} dV = \int_S (P_i + \Delta P_i) \delta u_i dS. \quad (8)$$

The integrations in (4) and (8) are carried out with respect to the same state of the body. Subtraction yields the incremental virtual work equation, which is also referred to as the equation of continued equilibrium:

$$\int_V (\Delta S^{\alpha\beta} X_{k,\alpha} + S^{\alpha\beta} \Delta u_{k,\alpha} + \Delta S^{\alpha\beta} \Delta u_{k,\alpha}) \delta u_{k,\beta} dV = \int_S \Delta P_i \delta u_i dS \quad (9)$$

So far, the equilibrium equations have been formulated in terms of the stresses and displacements (strains).

This system of equations is complimented with the incremental constitutive equations:

$$\Delta S^{\alpha\beta} = \mathcal{L}^{\alpha\beta\gamma\delta} \Delta E_{\gamma\delta} \quad (10)$$

The correct definition of the contravariant components $\mathcal{L}^{\alpha\beta\gamma\delta}$ of the moduli, which is of major importance for accurate analysis, will be discussed in detail in the next section. The increment in Green's strain is related to the displacement increment by

$$\Delta E_{\gamma\delta} = \frac{1}{2}(X_{k,\gamma} \Delta u_{k,\delta} + X_{k,\delta} \Delta u_{k,\gamma} + \Delta u_{k,\gamma} \Delta u_{k,\delta}) \quad (11)$$

Since the moduli $\mathcal{L}^{\alpha\beta\gamma\delta}$ are symmetric with respect to the last two indices, the combination of (10) and (11) leads to the expression for the stress increment in terms of the displacement increment:

$$\Delta S^{\alpha\beta} = \mathcal{L}^{\alpha\beta\gamma\delta} (X_{k,\gamma} \Delta u_{k,\delta} + \frac{1}{2} \Delta u_{k,\gamma} \Delta u_{k,\delta}) \quad (12)$$

Equations (9) and (12) are the governing equations for the increment. If the co-ordinate system is Cartesian at the start of the increment, the equations are simplified to

$$\int_V (\Delta S_{ij} \delta_{ki} + S_{ij} \Delta u_{k,i} + \Delta S_{ij} \Delta u_{k,i}) \delta u_{k,j} dV = \int_S \Delta P_i \delta u_i dS \quad (13)$$

and

$$\Delta S_{ij} = \mathcal{L}_{ijkl} (\Delta u_{k,l} + \frac{1}{2} \Delta u_{m,k} \Delta u_{m,l}) \quad (14)$$

The moduli \mathcal{L}_{ijkl} are not the usual classical 'small strain' moduli. See the next section for details.

At the end of the increment, the state variables need to be updated. Here an important difference arises between a formulation in terms of a general convected curvilinear co-ordinate system and a convected co-ordinate system which is Cartesian at the beginning of each increment. For the curvilinear system, the contravariant components of second Piola–Kirchhoff stress need only be corrected for volume changes in order to become the contravariant components of Cauchy stress:

$$\sigma^{\alpha\beta} = (S^{\alpha\beta} + \Delta S^{\alpha\beta}) / \mathbf{J} \quad (15)$$

where \mathbf{J} is the Jacobian of the deformation increment. Note that if the material behaviour is (approximately) incompressible, no transformation is needed.

In the initially Cartesian approach, the second Piola–Kirchhoff stress must be transformed to true (Cauchy) stress in the Cartesian co-ordinate system:

$$\sigma_{ij} = (\delta_{ik} + \Delta u_{i,k})(S_{kl} + \Delta S_{kl})(\delta_{jl} + \Delta u_{j,l}) / \mathbf{J} \quad (16)$$

Again the Jacobian will be equal to unity if the material behaviour is (approximately) incompressible. If at the start of each increment the co-ordinate system is curvilinear but distance-measuring, as is usually the case in beam and truss problems, other transformation rules apply, which, for brevity, will not be discussed here.

CONSTITUTIVE EQUATIONS

In this section the moduli that relate the increment in the (contravariant) components of second Piola–Kirchhoff stress to the increment in the (covariant) components of Green's strain will be derived.

For an elastic-plastic material, the total strain rate must be separated into an elastic and a plastic part:

$$\dot{E}_{\alpha\beta} = \dot{E}_{\alpha\beta}^{(e)} + \dot{E}_{\alpha\beta}^{(p)} \quad (17)$$

As was demonstrated by Hutchinson⁷ and Wang and Budiansky,⁸ a suitable expression for the relation between rate of stress and elastic strain rate is

$$\dot{\sigma}_{\alpha}^{\beta} = \mathcal{L}_{\alpha}^{\beta\gamma\rho(e)} \dot{E}_{\gamma\rho}^{(e)} \quad (18)$$

with $\dot{\sigma}_{\alpha}^{\beta}$ the rate of the mixed tensor components of Cauchy stress. The yield criterion can also be written in terms of the mixed components of Cauchy stress:

$$f(\sigma_{\alpha}^{\beta}) = 0 \quad (19)$$

and the associated flow rule is readily derived as

$$\dot{E}_{\alpha\beta}^{(p)} = \dot{\lambda} g_{\alpha\gamma} \frac{\partial f}{\partial \sigma_{\gamma}^{\beta}} \quad (20)$$

where $g_{\alpha\gamma}$ is the covariant metric tensor. The rate quantity $\dot{\lambda}$ depends on the work-hardening properties of the material. Inversion of equations (17)–(20) yields an elastic-plastic relationship of the type

$$\dot{\sigma}_{\alpha}^{\beta} = \mathcal{L}_{\alpha}^{\beta\gamma\rho(e-p)} \dot{E}_{\gamma\rho} \quad (21)$$

When the material is not at yield or is unloading, the constitutive equation has the form

$$\dot{\sigma}_{\alpha}^{\beta} = \mathcal{L}_{\alpha}^{\beta\gamma\rho(e)} \dot{E}_{\gamma\rho} \quad (22)$$

The remaining problem is to transform this equation into one of the type (10). This is achieved by transformation of the rate of Cauchy stress into the rate of second Piola-Kirchhoff stress with the relation

$$\dot{S}_{\alpha}^{\beta} = \dot{\sigma}_{\alpha}^{\beta} + g^{\gamma\rho} \dot{E}_{\rho\gamma} \sigma_{\alpha}^{\beta} \quad (23)$$

where $g^{\gamma\rho}$ is the contravariant metric tensor. Next the rate of the mixed stress components is converted into the rate of the contravariant stress components. The relation between the stress components itself can be written as

$$S^{\alpha\beta} = g^{\alpha\gamma} S_{\gamma}^{\beta} \quad (24)$$

or, alternatively, in order to obtain a symmetric expression for $S^{\alpha\beta}$,

$$S^{\alpha\beta} = \frac{1}{2}(g^{\alpha\gamma} S_{\gamma}^{\beta} + g^{\beta\gamma} S_{\gamma}^{\alpha}) \quad (25)$$

The rate form of this relation is

$$\dot{S}^{\alpha\beta} = \frac{1}{2}(g^{\alpha\gamma} \dot{S}_{\gamma}^{\beta} + g^{\beta\gamma} \dot{S}_{\gamma}^{\alpha} + \dot{g}^{\alpha\gamma} \sigma_{\gamma}^{\beta} + \dot{g}^{\beta\gamma} \sigma_{\gamma}^{\alpha}) \quad (26)$$

where S_{α}^{β} is replaced by σ_{α}^{β} because the current state is also the reference state. With the relations

$$g_{\alpha\gamma} g^{\gamma\beta} = \delta_{\alpha}^{\beta} \quad (27)$$

and

$$\dot{g}_{\alpha\beta} = 2\dot{E}_{\alpha\beta} \quad (28)$$

where δ_{α}^{β} is the Kronecker delta, equation (26) yields

$$\dot{S}^{\alpha\beta} = \frac{1}{2}(g^{\alpha\gamma} \dot{S}_{\gamma}^{\beta} + g^{\beta\gamma} \dot{S}_{\gamma}^{\alpha}) - (g^{\alpha\beta} \sigma^{\rho\beta} + g^{\beta\gamma} \sigma^{\rho\alpha}) \dot{E}_{\gamma\rho} \quad (29)$$

Combination of (22), (23) and (29) and use of the symmetry of (25) then leads to the final relation

$$\dot{S}^{\alpha\beta} = \mathcal{L}^{\alpha\beta\gamma\rho} \dot{E}_{\gamma\rho} \quad (30)$$

with

$$\begin{aligned} \mathcal{L}^{\alpha\beta\gamma\rho} = & \frac{1}{2} (g^{\alpha\eta} \mathcal{L}_{\eta}^{\beta\gamma\rho(e-p)} + g^{\beta\eta} \mathcal{L}_{\eta}^{\alpha\gamma\rho(e-p)} \\ & - g^{\alpha\gamma} \sigma^{\rho\beta} - g^{\beta\gamma} \sigma^{\rho\alpha} - g^{\alpha\rho} \sigma^{\gamma\beta} - g^{\beta\rho} \sigma^{\gamma\alpha}) + \sigma^{\alpha\beta} g^{\gamma\rho} \end{aligned} \quad (31)$$

This equation is a generalization of the equation presented in Reference 4. Equation (31) can be multiplied by a time increment Δt to form an incremental constitutive relation, which introduces an approximation. The relative error is of the same order of magnitude as the increment in strain. Since the strain increment is limited by accurate integration of the plasticity equations, this does not impose a new restriction. See also the next section.

If the co-ordinate system is Cartesian at the start of the increment, equation (31) takes the simplified form

$$\mathcal{L}_{ijkl} = \mathcal{L}_{ijkl}^{(e-p)} - \frac{1}{2} (\delta_{ik} \sigma_{jl} + \delta_{jk} \sigma_{il} + \delta_{il} \sigma_{jk} + \delta_{jl} \sigma_{ik}) + \sigma_{ij} \delta_{kl} \quad (32)$$

where $\mathcal{L}_{ijkl}^{(e-p)}$ are the elastic-plastic moduli for the usual small-strain analysis.

The presence of the last term in (31) and (32) causes the constitutive equations to be non-symmetric. However, if the deformations are (nearly) incompressible, which is usually the case for metal plasticity, the last term can be neglected and the constitutive equations remain symmetric.

INTEGRATION OF THE RATE EQUATIONS

As has become clear in the previous sections, three sources of nonlinearity may be distinguished in the large strain plasticity problem:

1. Geometric nonlinearities (large rotational effects), resulting in equations (9) and (12).
2. Material nonlinearities, as present in the usual constitutive equations (22).
3. Constitutive nonlinearities (large strain effects) which cause the additional terms in equations (31) and (32).

In order to obtain the solution to the finite element problem in an efficient way, the solution technique has to be well chosen. There are two main aspects to the solution process of the nonlinear finite element equations:

- (a) the integration of the rate equations to (eventually nonlinear) incremental equations, which will be discussed in this section;
- (b) the solution of the nonlinear incremental equations, which will be discussed in the next section.

The difference between the elastic-plastic rate equations used here and the usual small strain elastic-plastic rate equations is formed by the terms proportional to the stress in (31)/(32). These terms are readily added in an existing elastic-plastic finite element program. Use was made of the standard plasticity algorithms of the MARC program, as described in Reference 6. The large strain terms were added in explicitly linearized incremental form.

Some simple single-element tests were carried out to test the correctness of the integration procedures. The first test carried out was a uniaxial tensile test on a plane stress element. The element dimensions, the boundary conditions and the material properties are shown in Figure 2.

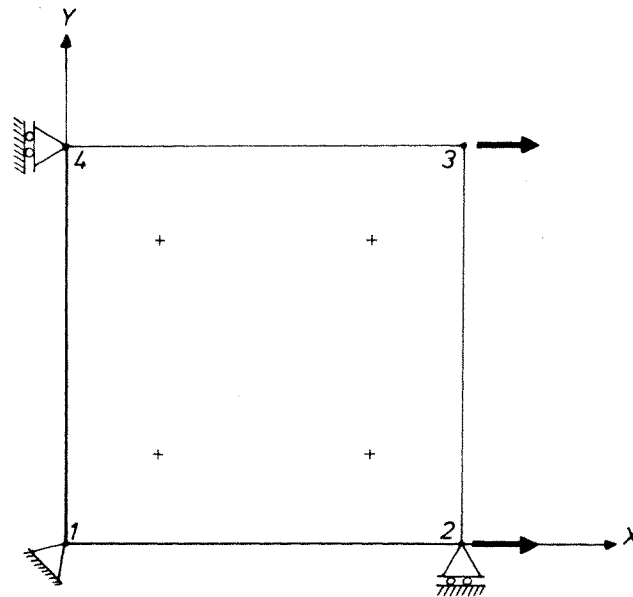
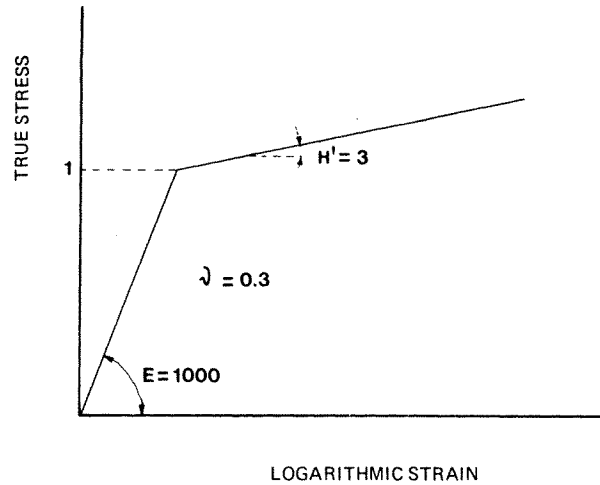


Figure 2. Uniaxial tension test, plane stress element

The usual J_2 -flow theory was used to form the elastic-plastic constitutive equations. The test was displacement-controlled, with equal displacement increments of 5 per cent of the original length. In Figure 3 the calculated true (Cauchy) stress is plotted as a function of the logarithmic strain $e = \ln(1 + u/l_0)$, where l_0 is the element length in the undeformed state. The drawn line in Figure 3 is the analytic solution for a rigid-plastic material with the same work-hardening characteristics:

$$\sigma = \sigma_y + h \ln(1 + u/l_0) \quad (33)$$

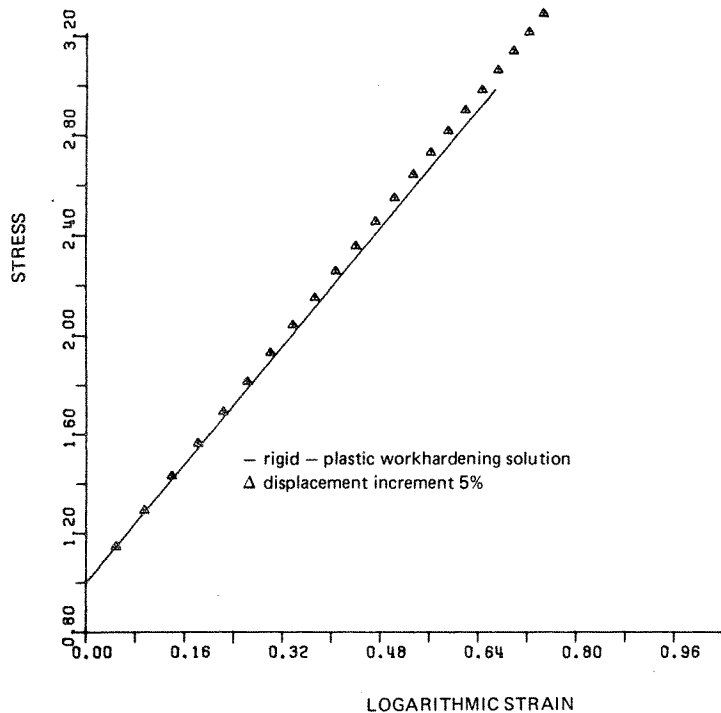


Figure 3. Uniaxial tension test, stress-strain diagram

The calculated stress differs slightly from the analytic solution, specifically for larger strains. This is attributable to the approximate integration of the rate forms (31)/(32) over finite increments of strain. As second test, the uniaxial tensile analysis was repeated with the same element, but now with controlled load, the load increments being equal to 5 per cent of the load to first yield. The results are shown in Figure 4, compared with the rigid-plastic analytical solution:

$$F = A_0[\sigma_y + h \ln(1 + u/l_0)]/(1 + u/l_0) \quad (34)$$

The test results are in good agreement with the analytical solution, except in the last increment, where the load actually increases to above the theoretical maximum. The last part of the analysis was subsequently repeated with load increments of 2.5 per cent. The results are also plotted in Figure 4, and an improvement in accuracy clearly shows.

In order to check the consistency of the formulation, the uniaxial test on the plane stress element was repeated with the stressed direction at 45 degrees to the X -axis (Figure 5). A plot of maximum principal stress vs. the logarithmic strain in two different integration points shows strong fluctuations of the stress (Figure 6), although the strain histories at the points are identical to at least four-digit accuracy. This clearly indicates some form of (numerical) instability. The test was repeated with a generalized plane strain element, where the strain perpendicular to the plane of the element was left free, and in this analysis no instability developed (Figure 6). This is due to different procedures for integration of the plasticity equations. For problems characterized by a three-dimensional stress state (such as the generalized plane strain analysis), the MARC program uses the so-called 'mean-normal' method as described by Rice and Tracey.⁹ In this method the flow law is chosen such that the yield criterion is satisfied exactly at the end of

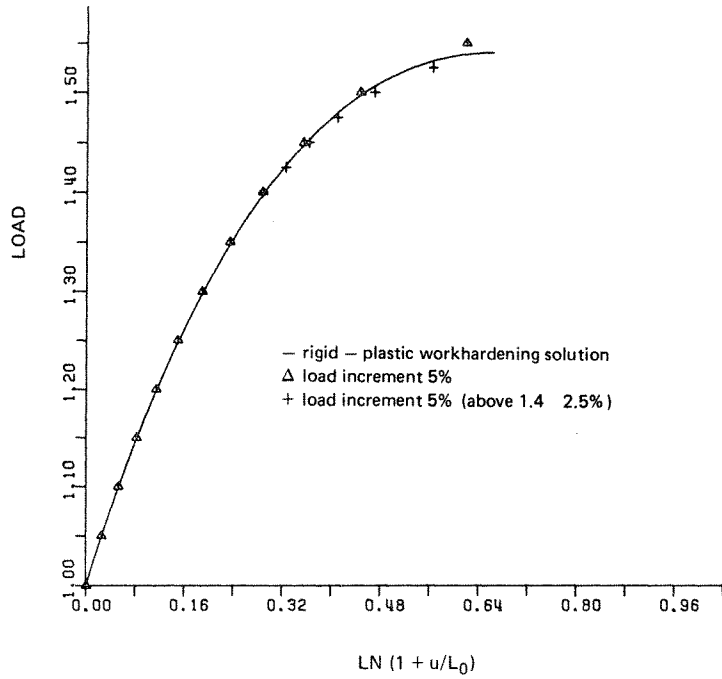


Figure 4. Uniaxial tension test, load-displacement diagram

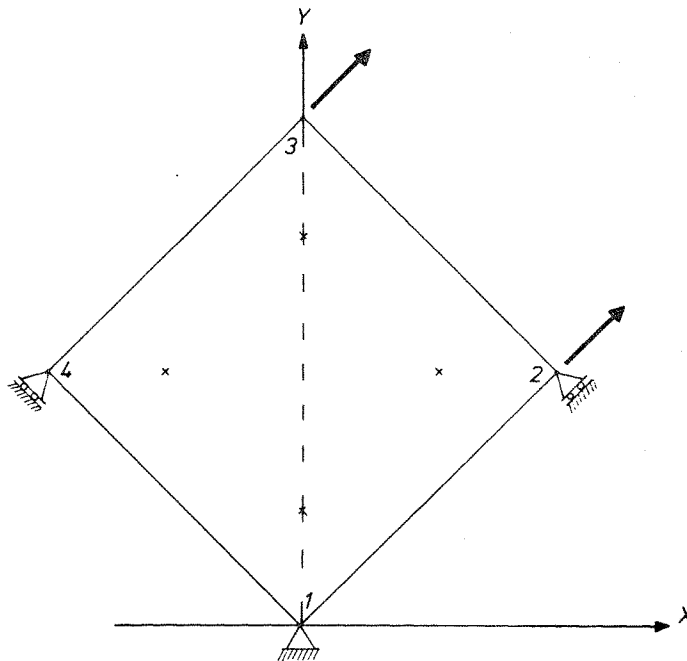


Figure 5. Uniaxial tension test, stressed direction 45 degrees

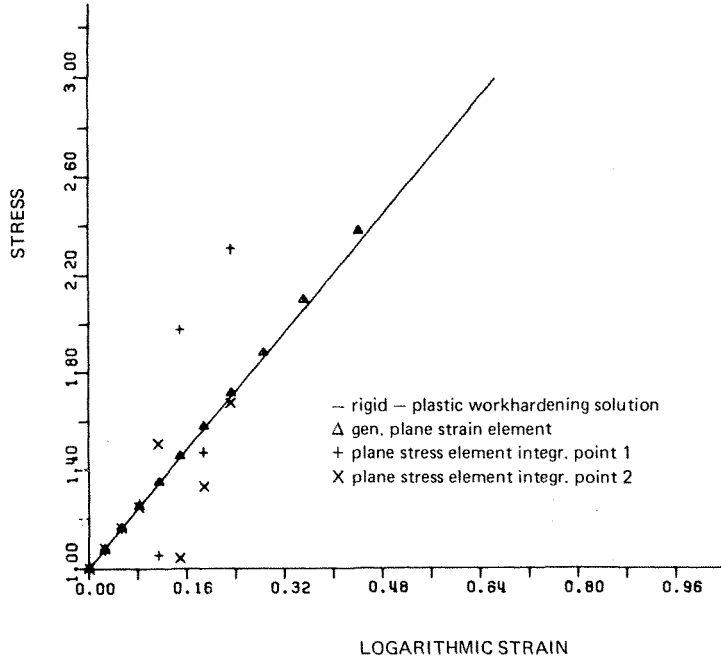


Figure 6. Uniaxial tension test 45 degrees, stress-strain diagram

the increment for a given increment in strain. For a state of plane stress, this method cannot be applied directly and the explicit tangent modulus method (with subsequent stress correction) is used. It is readily proved that the 'mean-normal' procedure is unconditionally stable, whereas the tangent modulus procedure has a clear stability limit for the strain increment. For a non-hardening material the proof is particularly simple. The elastic-plastic rate equation for such a material has the form

$$\dot{\sigma}'_{ij} = 2G \left[\dot{\epsilon}_{ij} + \frac{\lambda}{2G} \delta_{ij} \dot{\epsilon}_{kk} - \frac{3}{2} \frac{\sigma'_{ij} \sigma'_{kl}}{\sigma_0^2} \dot{\epsilon}_{kl} \right] \quad (35)$$

where σ'_{ij} is the deviatoric stress:

$$\sigma'_{ij} = \sigma_{ij} - \frac{1}{2} \delta_{ij} \sigma_{kk} \quad (36)$$

and σ_0 the equivalent (deviatoric) stress:

$$\sigma_0 = \sqrt{\frac{3}{2} \sigma'_{ij} \sigma'_{ij}} \quad (37)$$

From the rate equations (35), the tangent modulus method is obtained by substituting incremental values for the rates

$$\Delta \sigma'_{ij} = 2G \left[\Delta \epsilon_{ij} + \frac{\lambda}{2G} \delta_{ij} \Delta \epsilon_{kk} - \frac{3}{2} \frac{\sigma'_{ij} \sigma'_{kl}}{\sigma_0^2} \Delta \epsilon_{kl} \right] \quad (38)$$

Now consider a loading path for which the increment in strain is proportional to the deviatoric stress. Since the elastic strain increment vanishes, the flow rule yields

$$\Delta \epsilon_{ij} = \alpha \sigma'_{ij} \quad (39)$$

Consider an imposed strain increment that deviates slightly from (39):

$$\Delta \varepsilon_{ij} = \alpha (\sigma'_{ij} + \sigma''_{ij}) \quad (40)$$

where σ''_{ij} is a deviatoric stress tensor which is small compared to the equivalent stress and which is orthogonal to σ'_{ij} :

$$\sigma'_{ij} \sigma''_{ij} = 0 \quad (41)$$

Substitution of (40) in (38) yields

$$\Delta \sigma_{ij} = 2\alpha G \sigma''_{ij} \quad (42)$$

If another increment of the form (40) is applied, this increment may be written with respect to the stress at the start of the increment as

$$\Delta \varepsilon_{ij} = \alpha (\sigma'_{ij} + \Delta \sigma_{ij} + \sigma'''_{ij}) \quad (43)$$

where the deviation σ'''_{ij} is given by

$$\sigma'''_{ij} = \sigma''_{ij} - \Delta \sigma_{ij} = (1 - 2\alpha G) \sigma''_{ij} \quad (44)$$

The absolute value of the deviation increases and hence instability occurs if

$$\alpha > 1/G \quad (45)$$

or, when substituted in (39),

$$\Delta \varepsilon_{ij} > \sigma'_{ij}/G \quad (46)$$

The stability limit for the strain increment in this procedure is thus equal to twice the elastic strain up to yield. In the 'mean-normal' procedure, the incremental equations are formed in a different manner. In this procedure, a fictitious elastic mid-increment stress is defined:

$$\bar{\sigma}'_{ij} = \sigma'_{ij} + G \Delta \varepsilon_{ij} \quad (47)$$

and this stress is used in the formation of the incremental constitutive equation:

$$\Delta \sigma_{ij} = 2G \left[\Delta \varepsilon_{ij} + \frac{\lambda}{2G} \delta_{ij} \Delta \varepsilon_{kk} - \frac{3}{2} \frac{\bar{\sigma}'_{ij} \bar{\sigma}'_{kl}}{\bar{\sigma}_0^2} \Delta \varepsilon_{kl} \right] \quad (48)$$

where $\bar{\sigma}_0$ is the equivalent elastic mid-increment stress:

$$\bar{\sigma}_0 = \sqrt{\left(\frac{3}{2}\right) \bar{\sigma}'_{ij} \bar{\sigma}'_{ij}} \quad (49)$$

Let the strain increment again be defined by (40) and (41), and let σ''_{ij} be small compared to σ'_{ij} ; it then readily follows that

$$\Delta \sigma_{ij} = 2\alpha G \left[\sigma''_{ij} - \frac{\alpha G}{1 + \alpha G} \sigma''_{ij} \right] = \frac{2\alpha G}{1 + \alpha G} \sigma''_{ij} \quad (50)$$

For the next increment, the stress deviation σ'''_{ij} is given by

$$\sigma'''_{ij} = \sigma''_{ij} - \Delta \sigma_{ij} = \frac{1 - \alpha G}{1 + \alpha G} \sigma''_{ij} \quad (51)$$

Clearly, for all values of α between zero and infinity the absolute value of the deviation decreases. Hence, the 'mean-normal' procedure for integration of the elastic-plastic constitutive equations is unconditionally stable. The above derivations explain why, in the tensile test

carried out under 45 degrees, the generalized plane strain formulation is stable and the plane stress formulation is unstable.

The apparent stability in the first test turned out to be due to the complete absence of initial deviations σ''_i . The instability also occurs in the stress history in a plane stress element subjected to pure shear (Figure 7). The calculation was first carried out with the tangent modulus method, and after a few increments the stresses started to oscillate violently (Figure 8). The analysis was then repeated using the mean-normal method. As is clear from Figure 8, no instability develops in this calculation.

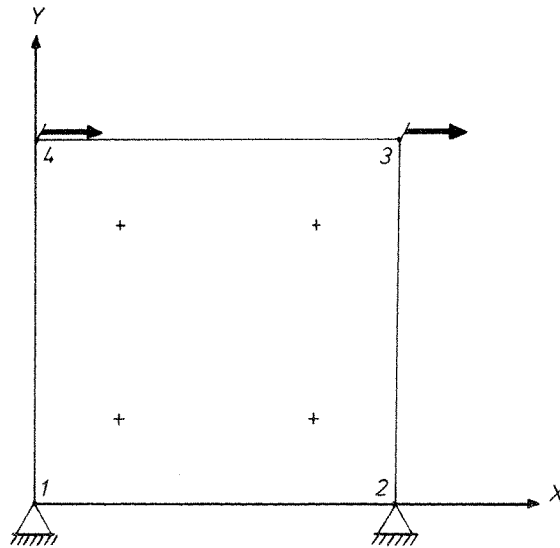


Figure 7. Pure shear test, plane stress element

The previous discussion has shown that a stability limit of twice the elastic strain exists for the strain increment in the explicit integration of the elastic-plastic constitutive equations. This stability limit does not exist for the 'mean-normal' integration procedure. For typical metal forming problems, the total strains are two to three orders of magnitude larger than the elastic strains. With a straightforward explicit tangent modulus procedure this means that several hundreds of increments have to be calculated, with in most cases very high computing costs. Nevertheless several analyses with a number of increments in this range can be found in the literature.^{10,11} The stability limit does not necessarily dictate the 'global' increment size; sub-incremental techniques presumably may be used successfully to overcome the stability problems. The disadvantage of such a procedure (and of the 'mean-normal' procedure) is its nonlinear nature, which requires an iterative solution scheme. A more elaborate study concerning the integration of the constitutive equations is certainly desired, and is planned by the authors.

SOLUTION OF THE INCREMENTAL EQUATIONS

In the previous section, the transformation of the rate equations into incremental equations was discussed. The nonlinearity of the incremental finite element equations depends strongly on this

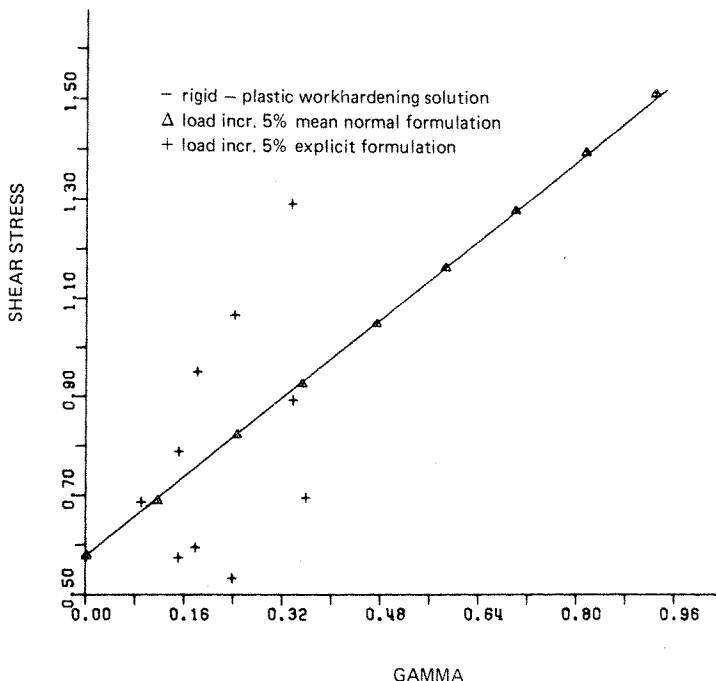


Figure 8. Pure shear test, stress-strain diagram

transformation. If the equations are formed by explicit linearization, the nonlinearity in the incremental equations is the same as the nonlinearity in the rate equations, and is only caused by the elastic-plastic loading/unloading effects. The disadvantage of such a simple linearization is the limited increment size due to accuracy and stability requirements.

In the present study, the incremental equations have been derived in a more accurate, but more nonlinear form. In particular, nonlinearities appear in the equations due to:

- (a) elastic-plastic loading/unloading effects;
- (b) the implicit 'mean-normal' formulation for plastic flow (48);
- (c) the exact implementation of the incremental virtual work equations (9), (13).

The solution of a system of nonlinear equations is a mathematical topic which can be discussed without reference to the methods used to generate the equations. Methods such as successive substitution, Newton(-Raphson) iteration, modified Newton iteration, quasi-Newton iteration, (conjugate) gradient method, etc., are described in textbooks on numerical analysis.¹² It is examined which of these methods are suitable to solve the finite strain plasticity equations. The elastic-plastic loading/unloading phenomena are treated effectively with a 'direct' iteration procedure. An initial guess is made as to which regions are loading and which regions are unloading. Subsequently the displacement increments are calculated and the actual loading/unloading regions are determined. If necessary, this calculation serves as the next guess, etc. Experience has shown that this procedure is straightforward and effective for problems with this type of nonlinearity.

The 'direct' iteration method is readily extended to cover the implicit 'mean-normal' formulation for plastic loading as well. An initial guess is made of the expected strain increment

$\Delta \varepsilon_{ij}$, and the corresponding (fictitious) elastic mid-increment stress $\bar{\sigma}_{ij}$ is calculated with equation (47). This stress is used in the formation of the incremental constitutive equation (48) that is used to calculate the incremental solution. This calculation provides the next guess, etc. Again, this procedure has proved to be quite effective for plasticity problems. Hence, a satisfactory solution has been obtained for problems (a) and (b).

Since two of the three nonlinear effects have been handled with a 'direct' iteration procedure, it appears logical to take care of the third effect in the same way. The formulation of this iterative procedure is derived from equations (9) and (12). If the superscript (n) denotes the results from the previous iteration, the results $(n+1)$ of the next iteration are obtained from the equations

$$\int_V [\Delta S^{\alpha\beta(n+1)} (X_{k,\alpha} + \frac{1}{2}\Delta u_{k,\alpha}^{(n)}) + (S^{\alpha\beta} + \frac{1}{2}\Delta S^{\alpha\beta(n)}) \Delta u_{k,\alpha}^{(n+1)}] \delta u_{k,\beta} dV = \int_S \Delta P_i \delta u_i dS \quad (52a)$$

$$\Delta S^{\alpha\beta(n+1)} = \mathcal{L}^{\alpha\beta\gamma\delta} (X_{k,\gamma} + \frac{1}{2}\Delta u_{k,\gamma}^{(n)}) \Delta u_{k,\delta}^{(n+1)} \quad (52b)$$

This method turns out to be not particularly effective, and performs rather poorly for slender structures, which is a disadvantage in the analysis of sheet metal forming problems. Instead of the direct iteration method, a full Newton-Raphson iteration can be included, and better performance may be expected for most practical problems. However this procedure is also only moderately effective for slender structures. The reason is the presence of nonlinear terms in the calculation of the strain increments (11). In slender structures, such as beams, the rotation increments are usually much larger than the strain increments, and hence the nonlinear terms in (11) may dominate the linear terms. Since the iteration procedures start with a fully linearized calculation of the displacement increments, the nonlinear contributions yield strain increments inconsistent with the calculated displacement increments in the first iteration. These errors give rise to either incorrect plasticity calculations, or, in the case of elastic material behaviour, yields erroneous stresses. These stresses in their turn have a dominant effect on the stiffness matrix for subsequent iterations or increments, which then causes the relatively poor performance.

The remedy to this problem is as simple as it is effective. The linear and nonlinear part of the strain increments are calculated separately and only the linear part of (11)

$$\Delta E_{\gamma\delta}^{(\text{lin})} = \frac{1}{2}(X_{k,\gamma} \Delta u_{k,\delta} + X_{k,\delta} \Delta u_{k,\gamma}) \quad (53)$$

is used for calculation of the stresses. The nonlinear part of (11)

$$\Delta E_{\gamma\delta}^{(\text{non})} = \frac{1}{2} \Delta u_{k,\gamma} \Delta u_{k,\delta} \quad (54)$$

is used as 'initial strain' in the next iteration or increment, which leads to an additional residual load vector $P_i^{(\text{res})}$ defined by

$$\int_S P_i^{(\text{res})} \delta u_i dS = \int_V \delta_{k,\beta} X_{k,\alpha} \mathcal{L}^{\alpha\beta\gamma\delta} \Delta E_{\gamma\delta}^{(\text{non})} dV \quad (55)$$

Since the displacement and strain increments are now calculated in a consistent way the plasticity and/or equilibrium errors are greatly reduced. Therefore it may be expected that the performance of the 'strain correction' method is better than the performance of the previously mentioned methods. The performance of the strain correction method is less if the displacement increments are (almost) completely prescribed, which is not usually the case. Finally note that the strain correction method can be considered as a Newton method, in which a different stiffness matrix is used. A mathematical examination of the strain correction method may provide better insight in its advantages and limitations.

As an illustration of the above methods consider the simple elastic cantilever beam in Figure 9. The beam is loaded by a bending moment M , to obtain a total rotation of the tip of 0.6 rad in six equal loading steps. With the direct iteration method no convergence is obtained, the full Newton method needs three iterations per step, and the strain correction method needs no iterations at all.

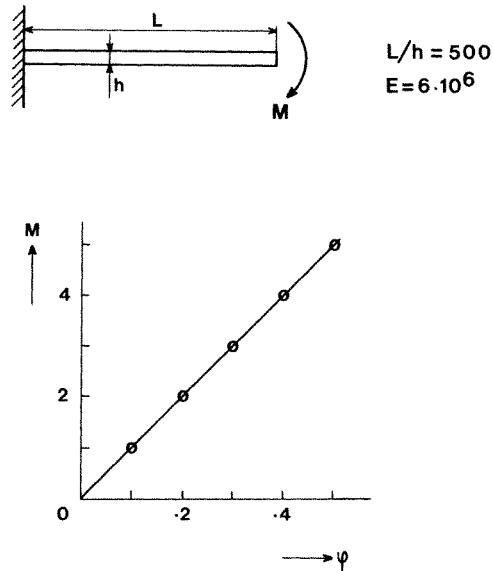


Figure 9. Cantilever beam subjected to bending moment

In order to test accuracy and stability of the implemented formulation two test problems, for which rigid-plastic workhardening solutions could be obtained, were calculated with different increment sizes. In both problems the 'mean-normal' formulation for plasticity and the strain correction method for geometric nonlinearity were used.

The first test problem was a thick-walled tube with inner radius 1 and outer radius 2 under internal pressure, with no strain in the axial direction. The material behaviour was assumed to be identical with the behaviour in the simple single-element tests. Five 8-node quadrilateral elements with reduced integration were used to model the tube. The total internal load $F_i = 2\pi r_i p_i$, where r_i is the current internal radius, was increased in equal increments. In the first analysis, the load was increased in steps of 5 per cent of the load to first yield. The result, presented as a pressure vs. internal radius diagram, is shown in Figure 10, together with the analytical solution for the rigid work-hardening material. The agreement obtained between theory and finite element calculations is excellent.

In the second analysis, the increment size was chosen four times as large as in the first analysis. From Figure 11 it is clear that the larger load steps do not cause a significant decrease in accuracy. It should be noted, however, that for the analysis with large increments the number of iterations for convergence of the (plasticity) equations has increased somewhat (average from 2.4 to 3.4 per increment).

Although this first test gives a good impression of the accuracy and stability of the integration of the constitutive equations in particular, it does not yield information about the nonlinear virtual work equations, since no rotations occur.

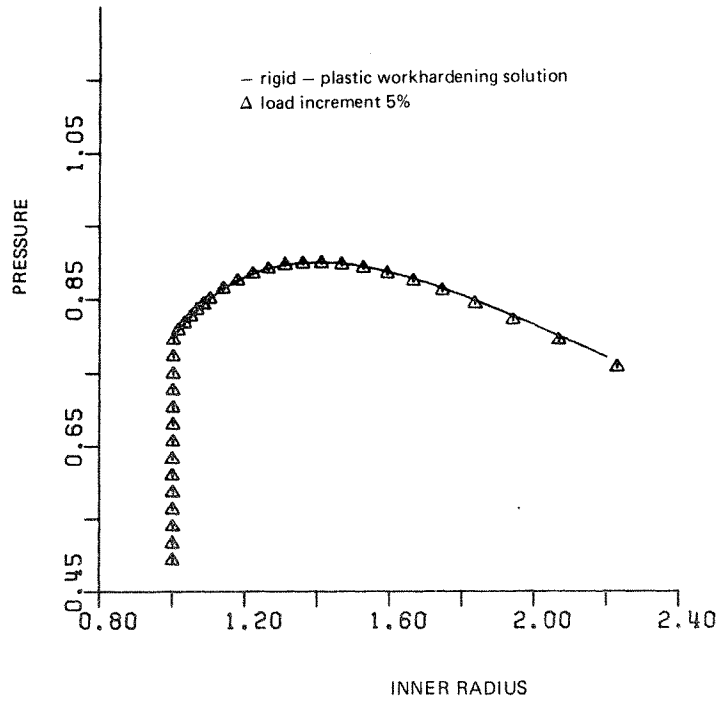


Figure 10. Thick-walled cylinder, 8-node quadrilateral elements. Diagram of pressure vs. internal radius, moderate load increment

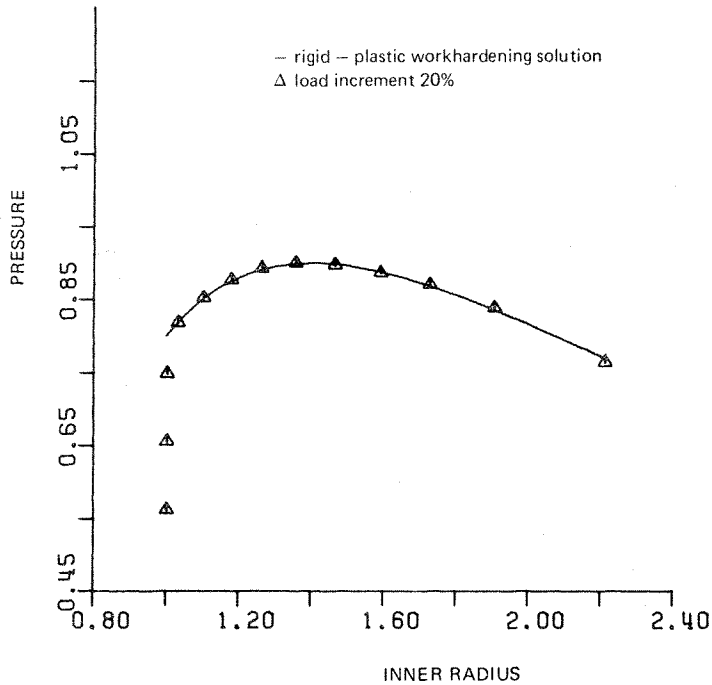


Figure 11. Thick-walled cylinder, 8-node quadrilateral elements. Diagram of pressure vs. internal radius, large load increments

A better evaluation of this aspect is made in the second test, the calculation of the in-plane torsion problem.¹³ The problem, the material properties and the finite element model are shown in Figure 12. The finite element model consists of a three degree fan of 4-node constant dilatation quadrilateral elements. Appropriate constraint conditions are enforced to ensure circular symmetry. The analysis was first run with small rotation increments (less than 3 degrees, Figure 13) and later repeated with large rotation increments (up to 6 degrees, Figure 14). Again the results are excellent in both cases, although some instability develops at the end of the large increment analysis. The in-plane torsion test is quite simple to analyse theoretically and

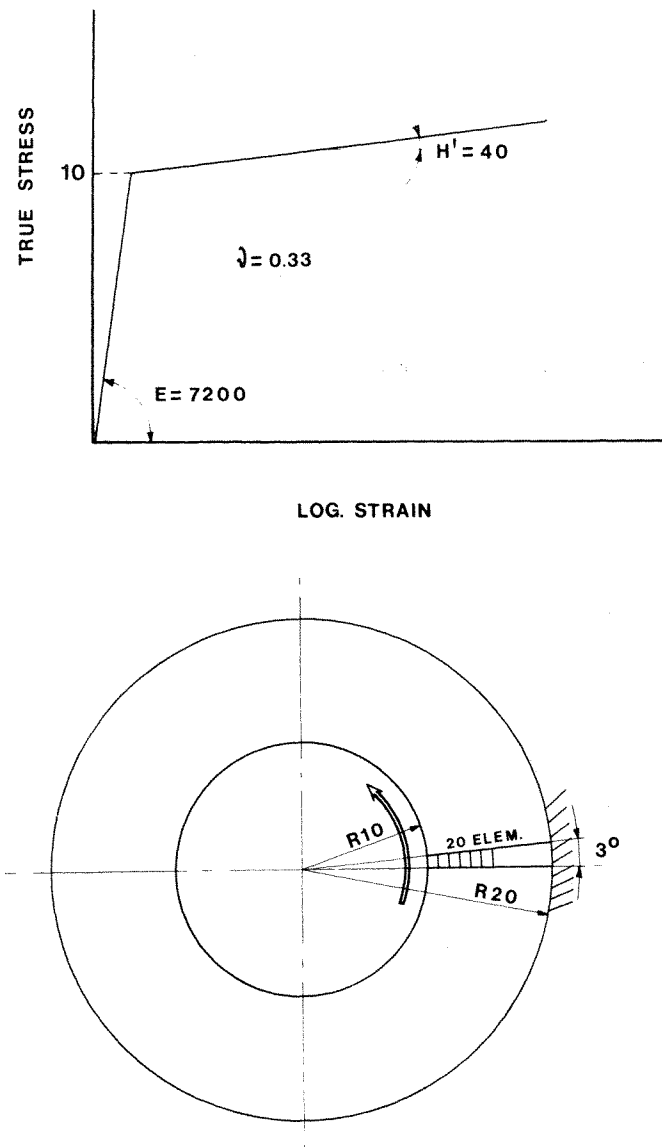


Figure 12. In-plane torsion test, 4-node quadrilateral plain strain element

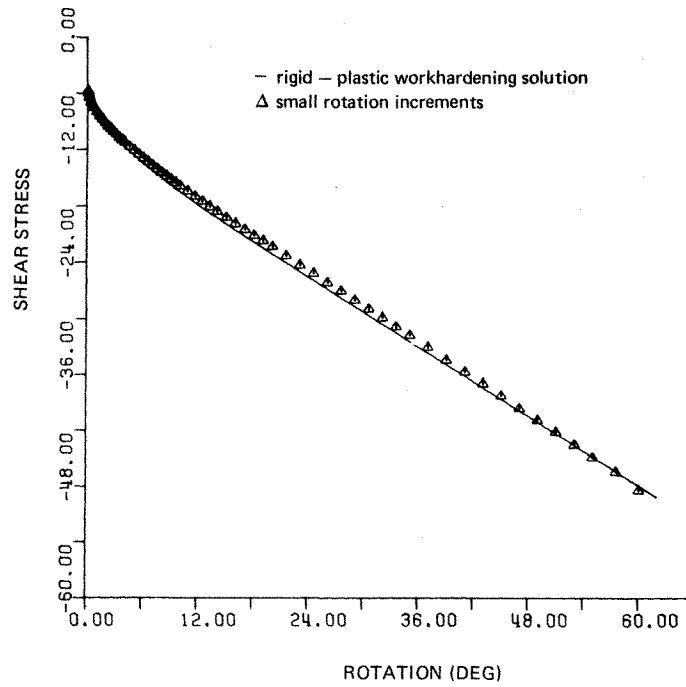


Figure 13. In-plane torsion test. Diagram of shear stress vs. rotation, small rotation increments

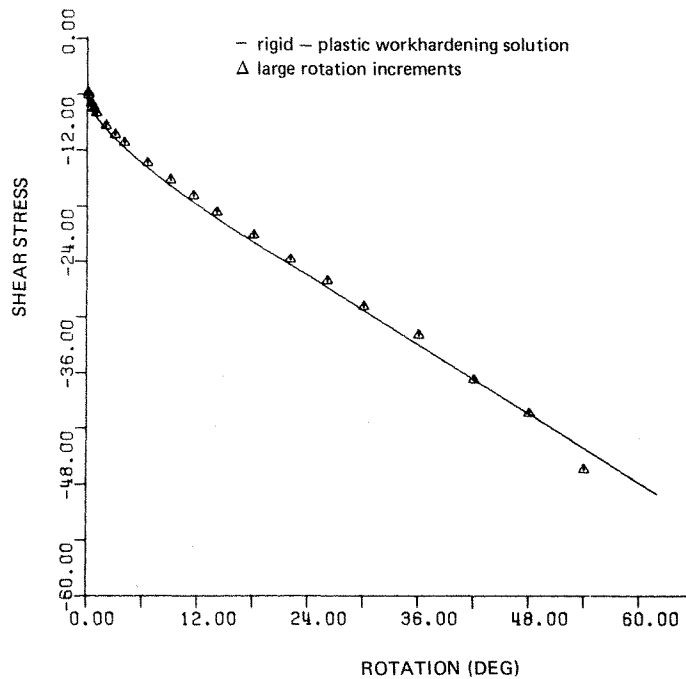


Figure 14. In-plane torsion test. Diagram of shear stress vs. rotation, large rotation increments

numerically, but it is actually a severe test for the algorithms used. The algorithms have to handle a combination of large strain, large rotation and a continuous changing stress state. At the end of the analysis, the shear strain at the inner radius is 105 per cent, and the directions of the principal stresses have rotated over 60 degrees. The fact that the deformations are indeed severe can be seen from the deformation history of the finite element mesh, shown in Figure 15.

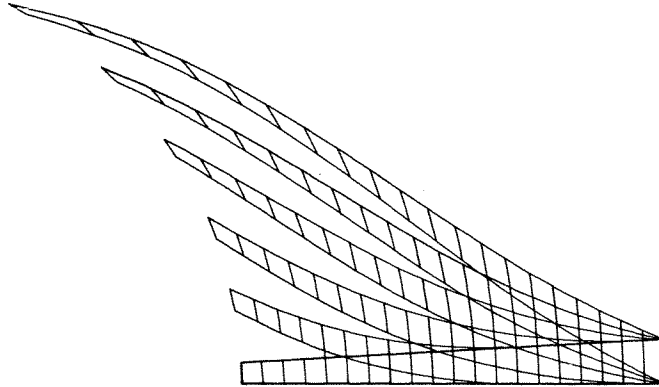


Figure 15. In-plane torsion test. Deformation history, rotation 10, 20, 32, 45, 60 degrees

SOME NOTES ON FINITE ELEMENT TYPES

Of considerable importance for the accurate calculation of large strain plasticity problems is the selection of adequate finite element types. In addition to the usual criteria for selection, two aspects need to be given special consideration:

1. The element types selected need to be insensitive to (strong) distortion.
2. For plane strain, axisymmetric and three-dimensional problems the element mesh must be able to represent non-dilatational deformation modes.

The last aspect has been discussed in detail in a paper by Nagtegaal, Parks and Rice,⁵ where it was shown that most finite element meshes tend to lock in the case of fully plastic material behaviour. As a remedy, a modified variational principle was introduced which effectively reduces the number of independent dilatational modes (=constraints) in the mesh. This procedure proved to be quite successful for plasticity problems in the conventional 'small' strain formulation. Zienkiewicz¹⁴ points out the positive effect of reduced integration for this type of problem, and demonstrates the similarity between modified variational procedures and reduced integration.

To test the performance of various element types, several problems are analysed with more than one element type. The first test problem was the thick-walled cylinder problem discussed in the previous section. The results with five 8-node quadrilateral reduced integration elements were shown in Figures 10 and 11. The analysis was repeated with five 8-node elements with full integration, and the results were found to be virtually indistinguishable from those obtained by means of reduced integration.

Subsequently the analysis was carried out with five 4-node quadrilaterals, both in the usual displacement formulation and in the constant dilatation formulation as presented in

Reference 5. The results are shown in Figure 16; the usual formulation behaves poorly for this problem, whereas the constant dilatation formulation follows the analytical solution exactly.

The second test problem was the axisymmetric upsetting of a disk. The dimensions of the disk and the meshes used are shown in Figure 17; the material properties are the same as in the uniaxial tension test (Figure 2). Fully sticking conditions were assumed between disk and tool. The analysis was carried out with the four element types used in the previous problem. The calculated load–displacement curves are shown in Figure 18. Again, the usual 4-node quadrilaterals show an excessively stiff behaviour. The deformed meshes after 18 per cent height reduction are shown in Figure 19(a, b). Note that with the usual displacement method no strain

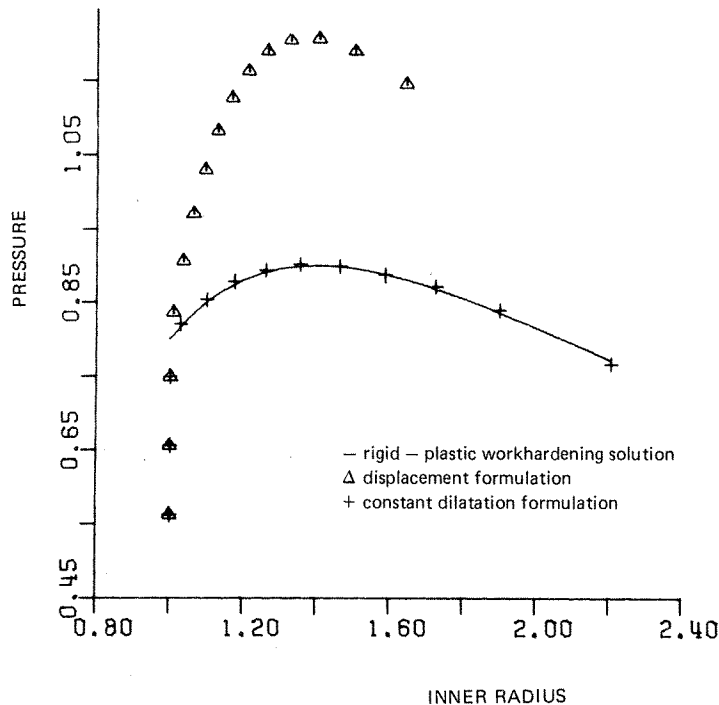


Figure 16. Thick-walled cylinder, 4-node quadrilateral elements, load increment 20 per cent

concentration forms near the edge of the disk, although such a strain concentration is observed in experiments. Of the 8-node quadrilateral elements, the fully integrated mesh also shows a (presumably) too stiff behaviour, although not as excessive as the 4-node element mesh. The reduced integration element mesh behaves less stiffly, but becomes as stiff as the fully integrated mesh in a later stage of the analysis. This effect can be explained from the deformed meshes after 18 per cent height reduction, Figure 20(a, b).

Whereas the fully integrated element mesh shows a similar lack of strain concentration as the 4-node quadrilateral mesh, the reduced integration element mesh shows a very peculiar deformation pattern near the edge. This strange pattern is due to dominance of the singular mode of the reduced integration element. Since an updated Lagrange method is used, the

element stiffness is formed in the distorted configuration of the element. The 8-node isoparametric elements are sensitive for the positions of the mid-side nodes. If these mid-side nodes are not in the middle between the corner nodes, linear strain variations over the element are not possible and the convergence rate decreases. This property is advantageous in the application of the so-called quarter-point node technique used to model the $1/\sqrt{r}$ singularity in fracture mechanics,^{15,16} but is a disadvantage in the current application. This automatically leads to the first additional requirement mentioned, the insensitivity to distortion. On the basis of the above

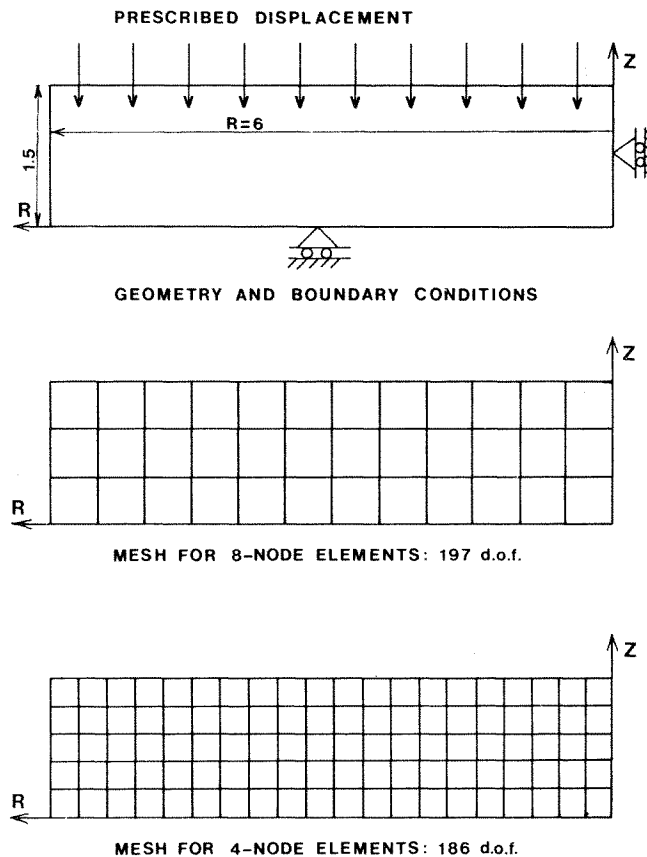


Figure 17. Axisymmetric upsetting, geometry and element meshes

experiences, it is concluded that for large strain plasticity calculations low-order elements are preferable to high-order elements. Consequently, all further calculations were carried out with 4-node isoparametric quadrilateral elements with constant dilatation.

Of course, in the case of excessive local distortion even the 4-node elements may fail to give good results; locally, the elements may even turn inside-out. In such excessive cases a periodic redefinition of the mesh seems to be the only possible solution to the problem. As yet, such techniques have not been explored. Finally it should be noted that the conclusions concerning the advantage of low-order elements only hold for continuum situations. Whether similar conclusions apply to shell or membrane problems remains an open question.

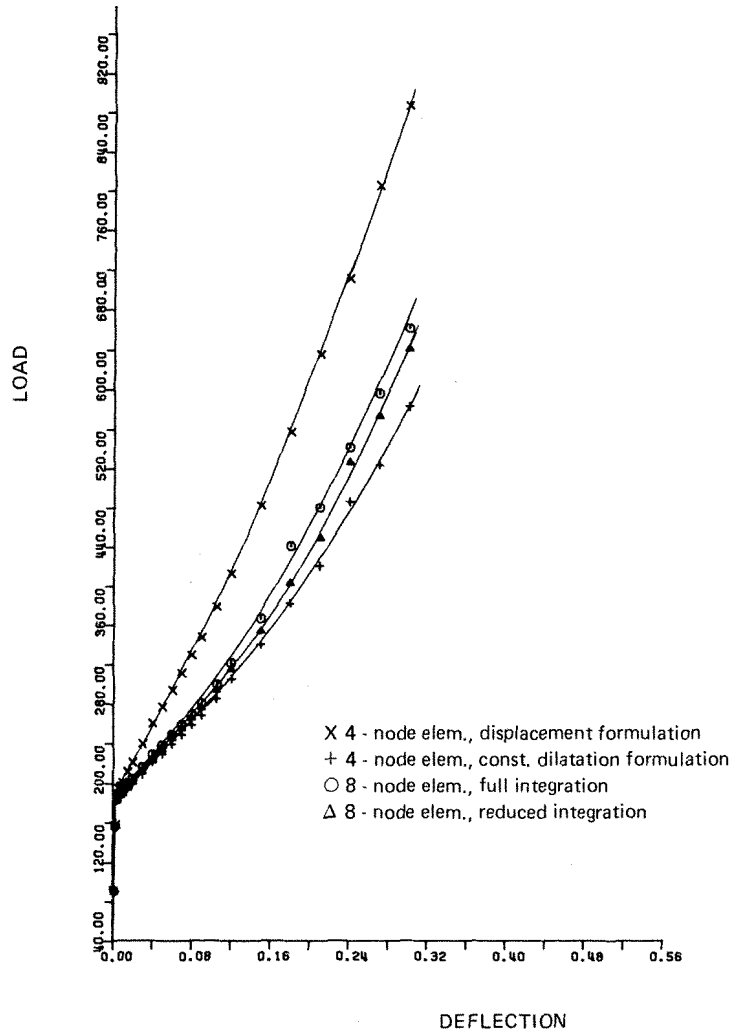


Figure 18. Axisymmetric upsetting, load-deflection diagram

COMPARISON WITH EXPERIMENTAL RESULTS

In order to compare the numerical results with experiments, two analyses were carried out for which recent experimental results were available. The first calculation concerned the axisymmetric upsetting of an aluminium disk. The disk, made of 99.7 per cent pure aluminium (specifications according to DIN code 3.0255.10), initially had a height of 0.8 mm and a diameter of 4.8 mm.

The stress-strain diagram is shown in Figure 21. In a paper by Brouha, de Jong and van der Weide¹⁷ detailed experimental results were presented, including displacement histories of numerous points on the disk-tool interface as well as the hydrostatic stress distribution on the interface at various stages of the process. The maximum height reduction was 64 per cent. Since no experimental data were available concerning the frictional behaviour between tool and

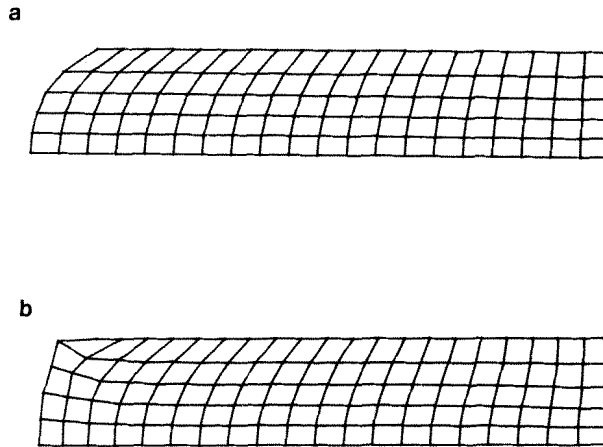


Figure 19. Axisymmetric upsetting, deformed meshes of 4-node elements: (a) displacement formulation; (b) constant dilatation formulation

specimen, the displacements in both the axial and the radial direction were prescribed along the interface. When the material deforms homogeneously, the increase in radius of a point with initial radius r_0 is equal to

$$\Delta r = R_0 \left[\left(1 - \frac{\Delta h}{h_0} \right)^{-1/2} - 1 \right] \quad (56)$$

where h_0 is the initial height and Δh the height reduction of the disk. The experimentally observed displacement curves on the interface were approximated with the equation

$$\Delta r = R_0 \left[\left(1 - \beta \frac{\Delta h}{h_0} \right)^{-1/2} - 1 \right] \quad (57)$$

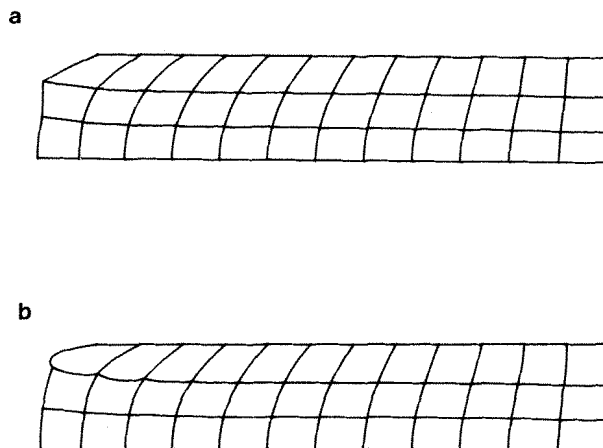


Figure 20. Axisymmetric upsetting, deformed meshes of 8-node elements: (a) fully integrated mesh; (b) reduced integrated mesh

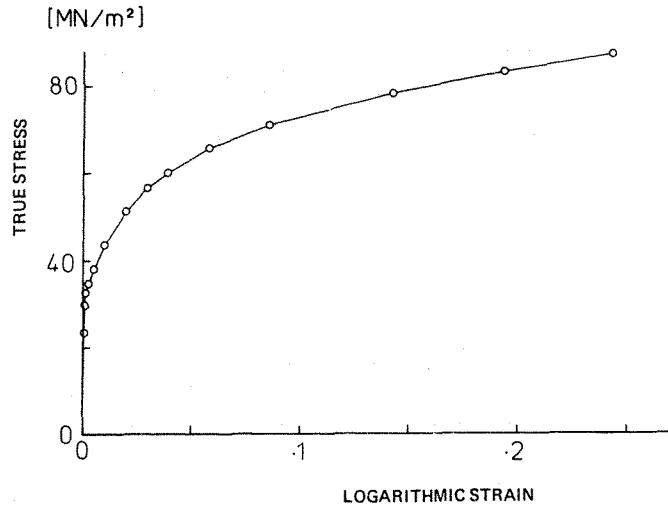


Figure 21. Axisymmetric upsetting with prescribed slip, stress-strain diagram

The best fit was obtained for $\beta = 0.87$. The deformed shape at 50 per cent height reduction is shown in Figure 22. The mesh shows strong distortion near the edges, which is in agreement with experimental observations. Experimentally and numerically obtained curves of the hydrostatic pressure are shown in Figure 23. The following differences clearly exist:

1. The overall level of the hydrostatic pressure in the analysis was higher than in the experiment.
2. In the experiment a local increase in pressure was measured near the centre of the specimen for reductions higher than 50 per cent. The analysis does not show this characteristic.

As yet, it is not possible to provide a satisfactory explanation for these differences; it is expected that the effects of friction are very important. A more elaborate study of this problem will be carried out in the near future.

The second problem deals with an actual manufacturing process. It concerns a flat plate in which a relatively small circular area is reduced in height. In this process, which is termed 'local upsetting' or 'coining', the maximum height reduction is 60 per cent. The ratio of tool radius to (initial) height is equal to three. The plate is made of CrNi steel with an initial yield stress of 52 MPa. Dry friction was assumed between tool and specimen, with the coefficient of friction

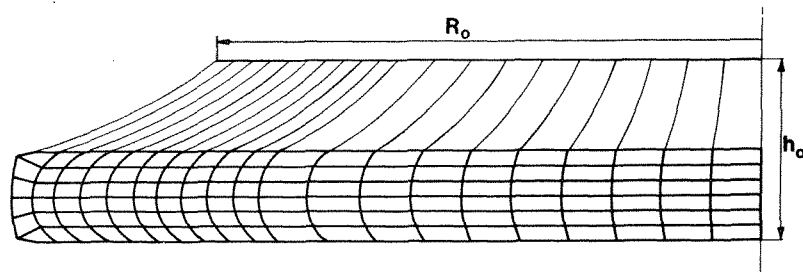


Figure 22. Axisymmetric upsetting with prescribed slip, deformed mesh at 50 per cent height reduction

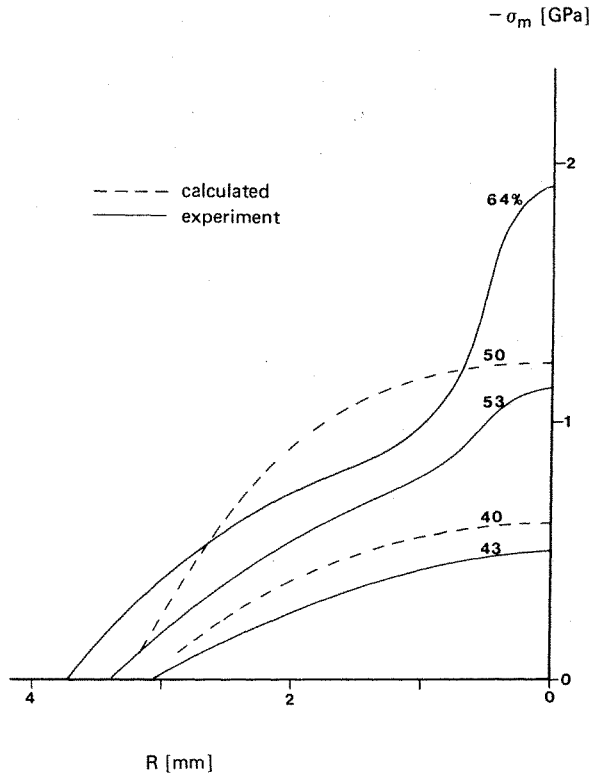


Figure 23. Axisymmetric upsetting with prescribed slip, hydrostatic pressure distribution at disk/tool interface

equal to 0.1. Perfect sliding conditions were assumed at the bottom of the plate. The experimental data available for this problem were considerably less extensive than for the previous problem, therefore the comparison between analysis and experiment is much less detailed.

The main results are displayed in Figure 24. There is a clearly noticeable bulging somewhat outside the tool radius. The shape and height Δh of this bulge are in good agreement with the

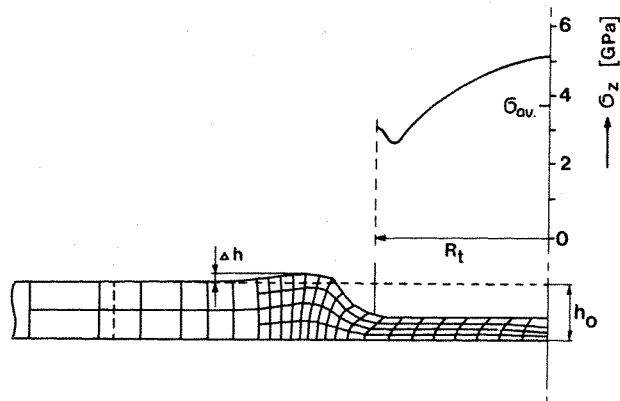


Figure 24. Coining, deformed mesh and pressure distribution on the tool

actual shape and height observed in the process. The average value of the stress σ_{av} on the tool of 3.8 GPa agrees well with the value deduced from the measured forging force.

In this process a substantial amount of energy is needed for the bulge formation. This results in a relatively high radial stress at the tool edge, which prohibits the development of a local strain concentration. Therefore the results of this calculation probably do not depend strongly on the assumptions made about the frictional behaviour between tool and plate. This may well explain the better agreement obtained between analysis and experiment in this second problem.

APPENDIX: LIST OF SYMBOLS

Latin indices refer to spatial (Cartesian) components.

Greek indices refer to material (convected) components.

Subscripts denote covariant components.

Superscripts denote contravariant components.

θ^α	= Convected material co-ordinates.
X_i	= Spatial position at start of increment.
x_i	= Spatial position at end of increment.
u_i	= Total displacement.
Δu_i	= Incremental displacement.
$\delta_{ij}, \delta_\alpha^\beta$	= Kronecker delta.
$g_{\alpha\beta}, g^{\alpha\beta}$	= Metric tensor.
$\delta\varepsilon_{ij}, \delta\varepsilon_{\alpha\beta}$	= Small strain variations.
$E_{ij}, E_{\alpha\beta}$	= Green (Lagrange) strain.
J	= Jacobian of the deformation-increment.
P_i	= Surface loads.
$\sigma_{ij}, \sigma^{\alpha\beta}$	= Cauchy stress.
$S_{ij}, S^{\alpha\beta}$	= Second Piola–Kirchhoff stress.
$\mathcal{L}_{ijkl}, \mathcal{L}^{\alpha\beta\gamma\delta}$	= Elastic–plastic moduli
$f(\sigma_\alpha^\beta)$	= Yield function.

REFERENCES

1. O. C. Zienkiewicz and P. N. Godbole, 'A penalty function approach to problems of plastic flow of metals with large surface deformations', *J. Strain Analysis*, **10**, 180–183 (1975).
2. G. C. Cornfield and R. H. Johnson, 'Theoretical predictions of plastic flow in hot rolling including the effect of various temperature distributions', *J. Iron and Steel Inst.* **211**, 567–573 (1973).
3. H. D. Hibbitt, P. V. Marçal and J. R. Rice, 'A finite element formulation for problems of large strain and large displacement', *Int. J. Solids Struct.* **6**, 1069–1086 (1970).
4. R. M. McMeeking and J. R. Rice, 'Finite-element formulations for problems of large elastic–plastic deformation', *Int. J. Solids Struct.* **11**, 601–616 (1975).
5. J. C. Nagtegaal, D. M. Parks and J. R. Rice, 'On numerically accurate finite element solutions in the fully plastic range', *Comp. Meth. Appl. Mech. Eng.* **4**, 153–177 (1974).
6. *MARC Programmers and Users Manual*, revision J, MARC Analysis Research Corporation, Palo Alto, California.
7. J. W. Hutchinson, 'Finite strain analysis of elastic–plastic solids and structures', in *Numerical Solution of Nonlinear Structural Problems* (Ed. R. F. Hartung), vol. 17, ASME, New York, 1973, pp. 17–29.
8. N. M. Wang and B. Budiansky, 'Analysis of sheet metal stamping by a finite-element method', *ASME J. Appl. Mech.* **45**, 73–82 (1978).
9. J. R. Rice and D. M. Tracey, 'Computational fracture mechanics', in *Proc. Symp. on Numerical and Computer Methods in Structural Mechanics*, Urbana, Illinois, 1971 (Ed. S. J. Fenves), Academic Press, New York, 1973, p. 585.
10. E. H. Lee, R. L. Mallett and W. H. Yang, 'Stress and deformation analysis of the metal extrusion process', *Comp. Meth. Appl. Mech. Eng.* **10**, 339–353 (1977).

11. P. Hartley, C. E. N. Sturgess and G. W. Rowe, 'A finite element analysis of extrusion-forging', Proc. 6th North American Metalworking Research Conf. Gainesville, Florida 1978, pp. 212-219.
12. G. Dahlquist and Å. Björck, *Numerical Methods*, Prentice-Hall, Englewood Cliffs, N.J., 1974.
13. R. Sowerby, Y. Tomita and J. L. Duncan, 'In-plane torsion testing of sheet metal', *J. Mech. Eng. Sci.* **19**, 213-220 (1977).
14. O. C. Zienkiewicz, *The Finite Element Method in Engineering Science*, 3rd edn, chap. xii, McGraw-Hill, London, 1980.
15. R. D. Henshell and K. G. Shaw, 'Crack tip finite elements are unnecessary', *Int. J. num. Meth. Engng.* **9**, 495-507 (1975).
16. R. C. Barsoum, 'On the use of isoparametric finite elements in linear fracture mechanics', *Int. J. num. Meth. Engng.* **10**, 25-37 (1976).
17. M. Brouha, J. E. de Jong and K. J. A. van der Weide, 'Experimental verification of finite element analysis on axial symmetric deformation processes', Proc. 7th North American Metalworking Research Conf., Ann Arbor, Michigan, 1979, pp. 57-64.